Near-Field Subsurface Electromagnetic Tomography and Holography

Konstantin P. Gaikovich
Institute for Physics of Microstructures RAS, GSP-105, Nizhny Novgorod, Russia, 607680
Nizhny Novgorod State University
Tel: (7831) 417 9468, Fax: (7831) 417 9464, e-mail: gai@ipmras.ru

ABSTRACT
Methods of multifrequency tomography and holography of subsurface dielectric inhomogeneities in the near-field zone based on the solution of inverse scattering problem are studied from the viewpoint of their applicability for targets with strong dielectric contrasts or with a complicated internal structure. Results based on numerical simulation with input data calculated from Maxwell equations are presented.
Keywords: electromagnetic inverse scattering problems, tomography, holography.

1. INTRODUCTION

Recently, a significant progress has been achieved in the region of the near-field electromagnetic tomography and holography of subsurface inhomogeneities [1-4]. Based on the electromagnetic perturbation theory, corresponding inverse scattering problems has been reduced to non-linear integral equations that can be solved iteratively using Tikhonov's method of generalized discrepancy [5,6] as linear Fredholm integral equations of the 1st kind at each step, beginning with the Born approximation. As it was demonstrated experimentally in [3], a subwavelength resolution in multifrequency scanning tomography can be achieved for targets buried in the near-field zone. However, there are serious limitations of such approach for large perturbations, when the Born approximation becomes poor as the first guess of iterative method.

To overcome these restrictions of perturbation theory, the new method of dual regularization based on the Lagrange approach in the optimization theory has been proposed to solve such problems using initial Maxwell equations [4], and results of this application to one-dimensional problems have demonstrated its ability to retrieve very strong variations of permittivity [7]. However, as it was obtained from our study, this method should be much optimized to be realized even with supercomputers. In this optimization, it is of prime importance to use a good first guess. In this paper, we study above-mentioned methods of tomography and holography to determine the range of their applicability in the Born approximation, at least, as a reasonable first guess for further, more rigorous, analysis. At that, methods are studied in numerical simulation based on direct calculations of scattered fields from Maxwell equation for various targets including those with a non-simply-connected inner structure. It was found that there is a wide enough region of targets' parameters where the solution in Born approximation gives reasonable results and is suitable for further corrections.

2. THEORY

If the scattering region is embedded in a medium with $\varepsilon = \varepsilon_0$, the subsurface complex permittivity can be written as $\varepsilon(\mathbf{r}) = \varepsilon_0 + \varepsilon_1(\mathbf{r})$. In Maxwell equations

$$\nabla \times \mathbf{E} = \frac{i\omega}{c}\mathbf{H}, \tag{1}$$

$$\nabla \times \mathbf{H} + i\frac{\omega}{c}\varepsilon_0\mathbf{E} = -i\frac{\omega}{c}\varepsilon_1\mathbf{E} + \frac{4\pi}{c}\mathbf{j} = \frac{4\pi}{c}(\mathbf{j}_{eff} + \mathbf{j}), \tag{2}$$

where ω is the frequency, c is velocity of light, it is possible to consider the first term in the right-hand side of (2) as an effective current source $j_{eff} = -i\frac{\omega}{4\pi}\varepsilon_1\mathbf{E}$ of the scattered field. Then, representing the total electric field as a sum of reference (probing) and scattered fields $\mathbf{E}(\mathbf{r}) = \mathbf{E_0}(\mathbf{r}) + \mathbf{E}_1(\mathbf{r})$, obtain the corresponding expression that solve the direct problem of electrodynamics from the Fredholm integral equation of the 2nd kind:

$$E_i(\mathbf{r}) = E_{0i}(\mathbf{r}) + E_{1i}(\mathbf{r}) = E_{0i}(\mathbf{r}) - \frac{i\omega}{4\pi}\int_{V'}\varepsilon_1(\mathbf{r}')E_j(\mathbf{r}')G_{ji}^{21}(x-x', y-y', z, z')d\mathbf{r}', \tag{3}$$

where $G_{ij}^{12} = {}^{\parallel}G_{ij}^{12} + {}^{\perp}G_{ij}^{12}$, $G_{ji}^{21} = {}^{\parallel}G_{ji}^{21} + {}^{\perp}G_{ji}^{21}$ are components of Green tensors that are sums of terms for TE ($\perp$) and TH($\parallel$) - polarizations; j_i is source current distribution (for brevity, we use mainly the same notations for

Fourier-transformations of these parameters). The convenient summation over repeated indices (*i, j = x, y, z*) is implied in (3).

The statement of inverse scattering problems can also be based on (1) considered as a non-linear integral equation of the 1st kind with a 6D kernel. The evident way is to begin the solution with the Born approximation:

$$E_{1i}(\mathbf{r}) = -\frac{i\omega}{4\pi}\int_{V'} \varepsilon_1(\mathbf{r}')E_{0j}(\mathbf{r}')G_{ji}^{lk}(x-x', y-y', z, z')d\mathbf{r}'. \tag{4}$$

As in has been proposed in [2], for the scheme of measurements with the fixed source-receiver vector $\boldsymbol{\delta}\mathbf{r}$, when the structure of the probing field is invariable relative to receiver position, (4) becomes a convolution equation, and can be reduced to a one-dimensional equation in *k*-space by 2D inverse Fourier transform over *x* and *y*:

$$\begin{aligned} E_{1i}(k_x, k_y, \omega, z, \boldsymbol{\delta}\mathbf{r}) = -4\pi^3 i\omega\int_{z'} \varepsilon_1(k_x, k_y, z')\{\int_{-\infty}^{\infty}\int_{-\infty}^{\infty} \mathrm{e}^{-i\kappa_x\delta x - i\kappa_y\delta y} \\ \times\int_{z''}[j_i(\kappa_x, \kappa_y, z''-z-\delta z, \omega)G_{ij}^{12}(\kappa_x, \kappa_y, z'', z', \omega)]G_{ji}^{21}(\kappa_x + k_x, \kappa_y + k_y, z', z, \omega)d\kappa_x d\kappa_y dz''\}dz', \end{aligned} \tag{5}$$

Based on the solution of (5), algorithms of microwave multifrequency tomography and perfect lens multilevel scanning tomography have been worked out and studied in numerical simulation [2]. To apply the multifrequency algorithm to real measurements, complex amplitudes of the received signal *s* are expressed by the convolution of the instrument function **F** of the receiver and the scattered field $\mathbf{E_1}$:

$$s(\mathbf{r}_r) = \int \mathbf{E}_1(\mathbf{r}')\mathbf{F}(x_r - x', y_r - y', z_r, z')dx'dy'dz', \tag{6}$$

where $\mathbf{r}_r$ is the vector determining the receiver position. It leads to a one-dimensional equation in *k*-space :

$$s(k_x, k_y, \omega) = \int_{z'} \varepsilon_1(k_x, k_y, z')K(k_x, k_y, z', \omega)dz, \tag{7}$$

However, it appeared difficult to recognize sounded subsurface objects on the measured image of $s(x, y, \omega)$ against the noise produced by the surface scattering [3]. Nevertheless, it was found that it is possible to obtain much better images of subsurface targets, using the transformation of multifrequency data to the synthesized pseudopulse [3]:

$$s(k_x, k_y, t) = \int_{\Delta\omega} s(k_x, k_y, \omega)\exp(i\omega t)d\omega, \tag{8}$$

that can be represented in dependence on the effective depth parameter z_s according $s(k_x, k_y, z_s) = s(k_x, k_y, t = -2z_s \operatorname{Re}\sqrt{\varepsilon_0}/c)$ (taking into account the light velocity in a medium and the signal path to and from a scattering element); the integration is over available frequency band $\Delta\omega$. It leads to the new equation that relates the complex permittivity spectrum to the complex-valued synthesized pseudopulse of the signal lateral spectrum:

$$s(k_x, k_y, z_s) = \int_{z'} \varepsilon_1(k_x, k_y, z')K_1(k_x, k_y, z', z_s)dz', \tag{9}$$

This transformation leads to the depth dependence of $K_1(k_x, k_y, z', z_s)$ with maxima that can explain the observed depth selectivity and resolution of pseudopulse images and provide better solution results in comparison with the exponential kernel of initial equation (7). To solve the Fredholm integral equation (9), the algorithm based on the generalized discrepancy principle in the complex Hilbert space W_2^1 [2] has been applied here to retrieve tomography images of subsurface inhomogeneities with the complex-valued distribution of permittivity. From the solution of (9), the desired 3D structure of permittivity (tomogram) is obtained by the 2D inverse Fourier transform:

$$\varepsilon_1(x, y, z) = \iint \varepsilon_1(k_x, k_y, z)\exp(ik_x x + ik_y y)dk_x dk_y. \tag{10}$$

Then, for a target with a homogeneous internal structure $\varepsilon_1 = \varepsilon_t$ it appeared possible to obtain the shape (*i.e.* to solve the problem of computer holography) using the inverse 1D Fourier transform of the *k*-space solution of (8) over one of its spectral parameters:

$$\varepsilon_1(k_y, x(x), z) = \int_{-\infty}^{\infty} \varepsilon_1(k_x, k_y, z)\exp(ik_x y)dk_y = f(k_y, x_1(y, z), x_2(y, z), z), \tag{11}$$

where, according the theory developed in [3], if the shape of a target can be expressed by two single-valued functions $x_1(y, z)$, $x_2(y, z)$ in each section *z = const*, the value $\varepsilon_1(k_x, x(y), z)$ is be expressed by these functions, and, using this expression as a complex-value transcendent equation (equivalent to the system of two real-valued

equations) one can obtain the shape of a sounded target. This system is overdetermined: it can be solved at each value of k_y. Using this fact, for targets with a non-simply-connected inner structure that include a single intrusion with $\varepsilon_1 = \varepsilon_{t2}$ described by two single-valued functions $x_3(y,z)$, $x_4(y,z)$, one can express (11) as

$$\varepsilon_1(k_y, x(x), z) = f(k_y, x_1(y,z), x_2(y,z), x_3(y,z), x_4(y,z), z) \tag{12}$$

and solve it as a system of two complex-valued equations at two different values of k_y to obtain these four functions.

3. RESULTS OF NUMERICAL STUDY

3.1 Direct calculations of scattered fields

As a first step to the solution of 3D inverse scattering problem based on Maxwell equations, the direct calculations of fields scattered by subsurface targets from (1), (2) has been carries out and applied in available algorithms of tomography. For a more general applicability, all lengths parameters are considered here as dimensionless (expressed in wavelengths). In Fig. 1, the near-field structure of the scattered field amplitude for a vertical incident plane wave is demonstrated in the vertical section *x*-*z* with sizes 1×1 (in wavelengths) for parallelepiped targets with sizes $0.2\times0.2\times0.15$. In Figs. 1a, 1b, results are given for targets with permittivity contrast $\varepsilon_1 = 3$ in a low-absorbing media; in Figs. 1c,1d – for absorbing targets with $\varepsilon_1 = 1+1.5i$ in an absorbing media with skin-depth $d_{sk} = 0.2$. In Figs. 1b, 1d, results are given for targets with an air-space (hollow) inside.

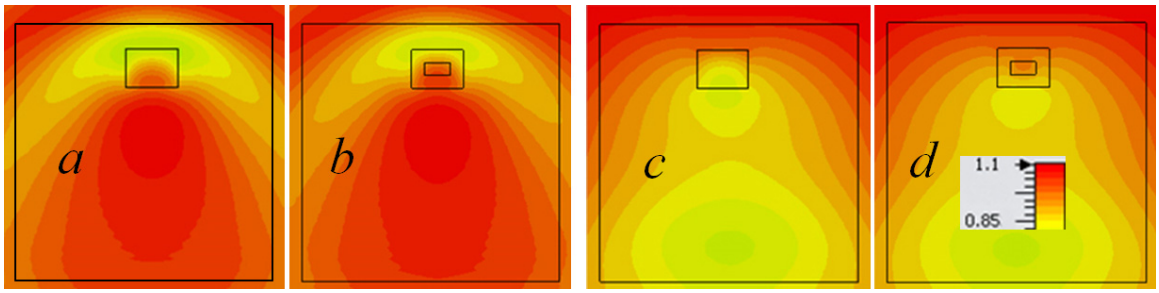

Figure 1. Structure of near-field scattering.

Results demonstrate that for considered targets the incident field isn't disturbed much (contrasts are less than 20%), so Born approximation could be valid in near-field diagnostics of such small targets, at least, as a first guess. This demonstration can be adjusted for various spectral ranges. For example, for wavelength of 500 nm, field pictures represent the scattered field from targets with sizes $100\times100\times75$ nm^3 in the region 500×500 nm^2; for microwave scattering at $\lambda = 20$ cm – for targets with sizes $4\times4\times3$ m^3. Even for ultra-low frequency 100 Hz that is used in earth crust sounding, distributions in Figs. 1c,1 d approximately reproduce the scattered field in the region 10×10 km^2 for inhomogeneities with sizes $2\times2\times1.5$ km^3 with conductivity of 4×10^{-4} Sm/m in a medium with skin-depth $d_{sk} = 3.6$ km. At fixed dielectric parameters, field disturbances grow with frequency, so that for inhomogeneities with sizes of about 0.5λ they typically can't be considered as small.

These field calculations have been applied in numerical simulation of near-field tomography and holography methods based on (9) and (11-12).

3.2 Numerical simulation of subsurface electromagnetic tomography and holography

As above, to simulate the proposed tomography quite generally, all spatial sizes are given in units of the longest wavelength λ_{max} in analysis. So, multifrequency measurements of signal complex amplitudes are simulated at 81 wavelengths in the wavelength band 0.2 – 1 (in our relative wavelengths units) for targets buried in a media with $\varepsilon_0 = 4+i$. In the simulation of tomography, signal complex amplitudes with the random gauss-distributed noise at *rms* 5% have been used in the analysis that have been calculated for the system of two identical transmitting and receiving antennas (with sizes 0.2×0.15 at the fixed distance between their centers of 0.35 and a homogeneous distribution of the current $\mathbf{j} = j_y\mathbf{y}$) placed in *y* direction and scanning together in the rectangle *x*-*y* area with sizes 1.5 × 1.5 above buried targets.

In Fig. 2a, the image of the calculated pseudopulse signal *s* at the value z_s= -0.2 for the parallelepiped sample with sizes $0.2\times 0.2\times0.15$ and $\varepsilon_1^0(\mathbf{r}) = 3$ (the same as in Fig. 1a) buried at depth *z* = -0.2 is shown. In Fig. 2b, the tomography result (distribution of real part of sample permittivity retrieved from the solution of (9)) is given in the horizontal section through the middle of the sample. In Fig. 2c, the holography image of a half of this target that is described by the function $x_1(y,z)$ obtained from (11) is shown.

In Fig. 2d, 2e, 2f, corresponding results are given for a target with a hole (with the same shape and permittivity as in Figs. 1b). The holography image in Fig. 2f is obtained by combing images for outer shape function $x_1(z, y)$ and hole shape function $x_3(z, y)$ obtained from (12).

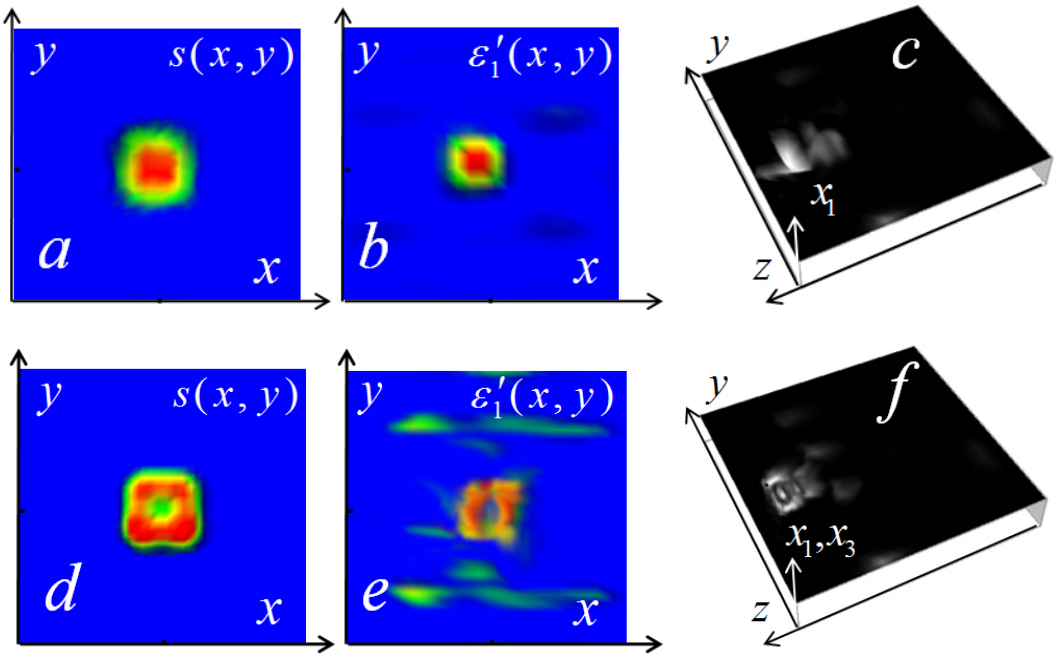

Figure 2. Results of numerical simulation. (a ,b, c), results for the target in Fig.1a; (d, e, f), results for the target in Fig. 1b. (a, c), images of pseudopulse signal; (b, e), tomography results in the horizontal section through the middle of targets; (c, f), holography images of targets (left halves).

One can see in Fig. 2 that results of tomography and holography simulation are in a reasonable correspondence with parameters of simulated targets. In holography images, some excessive details are seen that are possibly related to influence of the secondary scattering.

Results demonstrate that even for targets with considerable dielectric contrasts the studied near-field diagnostics based on the Born approximation can give reasonable results.

4. CONCLUSIONS

Methods of subsurface near-field electromagnetic tomography and holography that are based on the solution of the integral equation in Born approximation have been studied in numerical simulation. It was found that there is a wide region, where for inhomogeneities, small in comparison to probing wavelengths, perturbations of scattered field are small enough to apply methods. In such cases, this solution can be used in further analysis in more rigorous algorithms as a reasonable first guess.

ACKNOWLEDGEMENTS

This work was supported by Russian Foundation for Basic Research, grants *No*. 13-07-97028_r, 13-02-12155_ofi_m), and by the program of Russian Academy of Sciences.

REFERENCES

[1] K.P. Gaikovich: Subsurface near-field scanning tomography, *Physical Review Letters*, 2007, vol.98, 183902.

[2] K.P. Gaikovich and P.K. Gaikovich: Inverse problem of near-field scattering in multilayer media, *Inverse Problems*, vol. 26 pp. 125013, 2010.

[3] K.P. Gaikovich, P.K. Gaikovich, Ye.S. Maksimovitch, and V.A. Badeev: Pseudopulse near-field subsurface tomography, *Physical Review Letters*, vol. 108, pp. 163902, 2012.

[4] K.P. Gaikovich: Inverse scattering problems in subsurface diagnostics of inhomogeneous media (invited), *in Proc. ICTON 2013*, Cartagena, Spain, June 2013, paper Tu.D5.3.

[5] A.N. Tikhonov: *Solution of Ill-Posed Problems*, New York: Winston, 1977.

[6] K.P. Gaikovich: *Inverse Problems in Physical Diagnostics*.–New York: Nova Science Publishers Inc., 2004.

[7] K.P. Gaikovich, P.K. Gaikovich, and M.I. Sumin: Inverse scattering problem in pseudopulse diagnostics of periodic structures, in *Proc. 4th Int. Conf. on Mathematical Methods in Electromagnetic Theory* (Kharkiv, Ukraine, Aug. 2012), 390.